Pulsed NMR: Measurement of Relaxation Times

Samuel James Bader
MIT Department of Physics
(Dated: November 17, 2012)

We discuss the theory of NMR and demonstrate the measurement of T_1 and T_2 relaxation times in aqueous glycerin solutions with spin echo techniques. Using these results, we confirm Bloembergen's power-law relation between T_2 and viscosity, and discuss the utility of the experiment for precise magnetic field determination.

I. NMR AND SPIN ECHOS

Nuclear Magnetic Resonance serves as an important technique in many fields, including medicine (where it is known as MRI), chemical spectroscopy, and even quantum computation research. At its most basic, NMR is about the coherent manipulation and observation of nuclear dipole moments. Our work here deals exclusively with the hydrogen nucleus, which, being merely one proton, is both the simplest example and one of the most common nuclei in NMR.

The standard NMR configuration (Figure 1) places a macroscopic sample (in our case, a small vial of aqueous glycerol) in a strong magnetic field $B_0\hat{z}$ (for us, $B_0 \sim 1750G$). We begin in thermal equilibrium: the magnetic dipole moments $\vec{\mu}$ prefer to align with the magnetic field, but, at room temperature, the alignment energy is vastly outscaled by available thermal energy, so there is only a slight directionality. In a macroscopic sized sample, this will result in a detectable net magnetization along $\hat{z}$. Furthermore, as one can easily show, the magnetic dipole moments of the nuclei will precess with the Larmor frequency $\omega_0 = \gamma B_0$ around the magnetic field (at ∼7MHz for our parameters). But, since the dipole moments are in general out of phase, this results in no (initial) net magnetization in tranverse (x-y) plane.

As discussed in [5], the sample magnetization can be manipulated by application of a small oscillating transverse magnetic field $\vec{B_1} = B_1 \sin(\omega t)\hat{x}$. If the driving frequency ω is near resonance with ω_0 (typically, $|\omega - \omega_0| \sim$10 kHz), then the pulse can coherently rotate the dipole moment along the polar angle, by an amount proportional to the duration of its application (typically tens of μs). Most commonly, we will choose pulses to acheive π or $\pi/2$ rotations, and observations of the oscillating magnetic moment are made along the $\hat{x}$ direction.

The relaxation times of the system determine how long one can mantain coherent control over the magnetization. The spin-lattice relaxation, T_1, describes the timescale for thermal reequilibriation, the recovery of the system's original longitudinal magnetization after a pulse. The spin-spin relaxation, T_2, describes the timescale for transverse decoherence due to the interactions of neighboring spins; this coupling induces relative phase differences, reducing coherence and shrinking the net magnetization.

However, in practice, one actually observes a transverse decay time T_2^* much faster than these physically interesting relaxations. Due to the inhomogeneity of the static magnetic field, molecules distributed throughout the sample have different individual Larmor frequencies, and so, precessing at different rates, quickly lose coherence. However, assuming the molecules do not diffuse quickly, this decoherence can be reversed to allow observation of the interesting relaxations. The technique for this purpose is the *Han spin echo*: apply a $\pi/2$-pulse to rotate the magnetization down to the transverse plane, wherein it precesses and decoheres as faster spins separate from the slower spins during a wait time τ (typically in ms). Then apply a π-pulse to flip the magnetization: now the faster spins are "behind," and the slower spins "ahead." After another τ of waiting, all the spins will ideally converge back upon each other, and we witness an *echo* of the magnetization. In the echo, the T_2^* effect has been undone, and the magnetization is decreased only due to T_1 and/or T_2 decay.

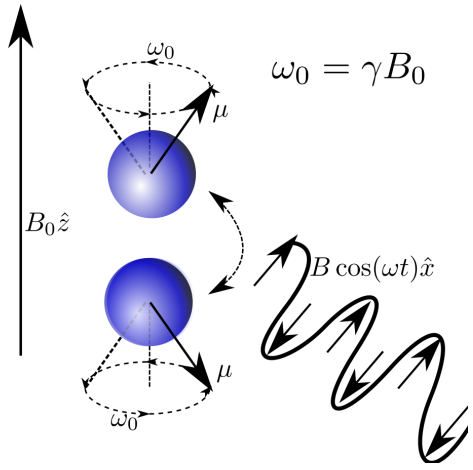

FIG. 1: Application of a resonant transverse B-field can rotate the magnetization.

II. EXPERIMENTAL SETUP

Our experimental set-up is provided in Figure 2. The sample is inside of an inductor coil, with a strong mag-

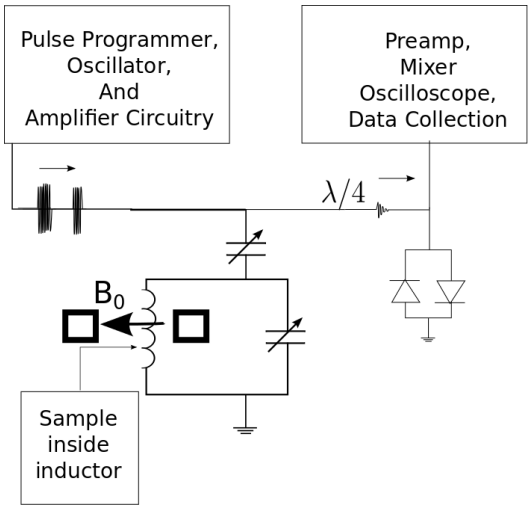

FIG. 2: The pulse-train from the programmer (top-left) travels to the inductor coil (middle). When not pulsing, the signal from the coil is amplified and collected from an oscilloscope (top-right).

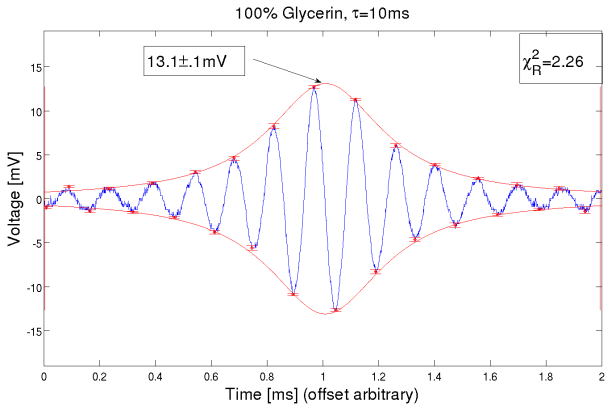

FIG. 3: A sample spin echo. The blue curve is raw data, the red points indicate automatically selected peaks, and the red curve represents a fitted Lorentzian.

netic field ($B_0 = 1750 \pm 20$G) across it, perpendicular to the inductor plane. From the top-left, there is a pulse programmer, which signals for switches gating the output of an Agilent 33120A Frequency Synthesizer. The resulting pulse train is amplified, fed through a pair of crossed diodes to reduce dark noise, and sent to the middle LC circuit. The pulses across the inductor produce the oscillating transverse magnetic field for the sample. Variable capacitors allow one to tune the LC circuit to resonate at the desired frequency and match the LC characteristic impedance to the line.

The transverse oscillations of the magnetization in the sample also create an oscillating B-field, which, when not pulsing, can be picked up by the inductor. This signal traverses the $\lambda/4$ line and the parallel crossed-diodes and arrives at the top-right, where it is mixed down with the pulse frequency, amplified, and collected from an oscilloscope. (The intermediate circuitry prevents the large pulses from reaching the sensitive pre-amp inputs).

III. ECHO FITTING

Each spin echo (eg Figure 3) which we collected was captured and digitally analyzed. From the raw data (blue curve), one can see a sinusoidal oscillation (at frequency $|\omega - \omega_0|$) with an envelope that is the echo itself. First the data is shifted to have mean zero, approximately eliminating any DC bias. Secondly, the oscillatory peaks (red points) are automatically selected from a smoothed dataset. The raw data has a resolution of 1μs, and peak height uncertainties were estimated from local standard deviations of the height within 5μs about a point.

Then, to determine the height of the spin echo, these peaks were fitted to a Lorentzian envelope. The Lorentzian is not theoretically justified, but generally fits the data reasonably well. In fact, theory would predict a rising exponential followed by decaying exponential; however, imperfections would round out the peak and noise prevents the wings from reaching zero too quickly, so we see something more like the above. In fact, both Lorentzian and exponential fits were attempted, and what we found was that, although the exponential fit tended to provide echo heights significantly heigher (∼14%), the two were generally in a definite ratio, with about 1% variation. Since we care about the decay of the signal, not its absolute scale, the choice of exponential or Lorentzian fit should thus be inconsequential for the final results. The 1% variation we will take as an additional uncertainty upon our fitted echo heights.

IV. T_1 AND T_2 DETERMINATION

T_2 decay applies only to transverse magnetization. Reviewing the procedure for a spin echo, we see that the magnetization should lie in the transverse plane for the entire procedure of time 2τ, where τ is the spin echo wait time. Assuming that T_1 is sufficiently larger than T_2, then varying τ should give us a decay of echo height which goes as $\exp[-2\tau/T_2]$. The T_2 decay for 100% glycerin is shown in Figure 4.

T_1 decay applies to the recovery of longitudinal magnetization. The three-pulse procedure for observing a T_1 curve is as follows. First, apply a π-pulse to flip the magnetization down, and wait a time τ for the magnetization to partially revert. (It should shrink from the $-\hat{z}$ direction to zero, and grow back to the equilibrium value in the $+\hat{z}$ direction). Then apply a spin echo sequence (with a small wait time relative to this τ), to flip the magnetization into the transverse plane and measure it. Since we only measure the magnitude of the echo height, with no information about which direction the magnetization was facing, we should expect to see a curve of the

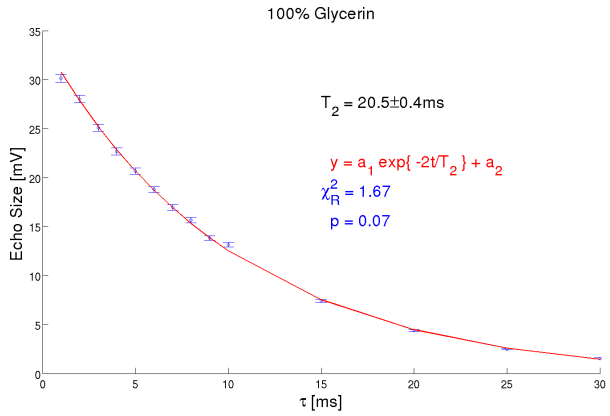

FIG. 4: We expect an exponential decay in τ of transverse magnetization. (A small additive term is included for any leftover DC biasing offset.)

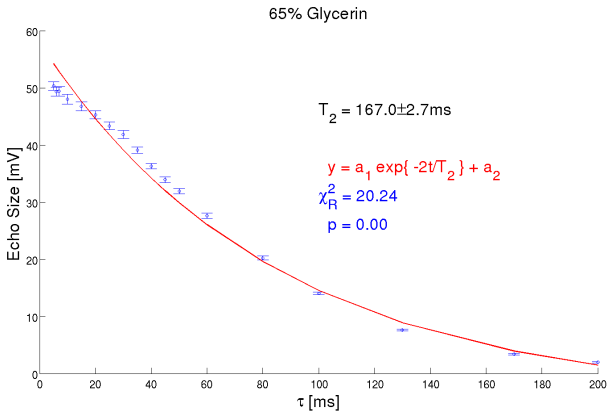

FIG. 6: The determinations of T_2 for lower concentration samples are untrustworthy. Notice the clear residual structure.

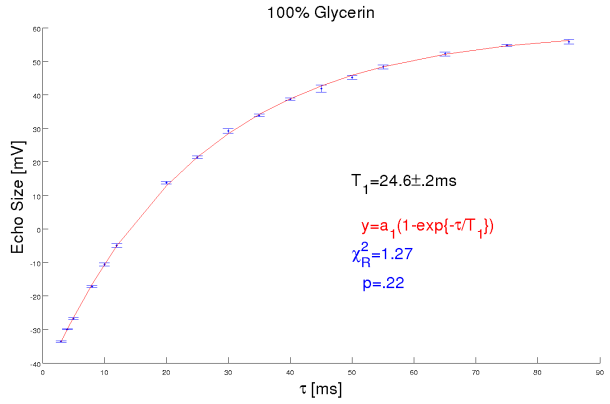

FIG. 5: We see a return to the equilibrium magnetization. The fitted T_1 is comparable to the 23ms listed [1] for a 10P glycerin solution

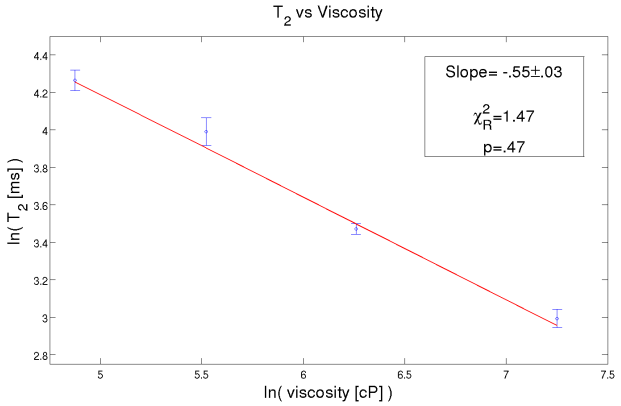

FIG. 7: The T_2-viscosity relation is well-described by a power law.

form $|1 - 2\exp[-\tau/T_1]|$. By observing where the curve reverses direction, we can reimpose the correct signs and get a final curve of the form $1 - 2\exp[-\tau/T_1]$. This relaxation curve is shown in Figure 5.

The T_1 determinations are generally solid fits like the one shown in Figure 5 with no significant systemic deviation. The higher percentage T_2 fits (above 75%) are similarly excellent, but, at the lower concentrations, the fits become less accurate, and we notice an obvious systemic residual structure, as shown in Figure 6. Fortunately, because the higher-concentration fits are so solid, we will still be able to observe the behaviour of T_2 clearly (at least at higher viscosities). We will thus discard the low concentration data for the next part of the discussion, and discuss the possible reasons in the following section.

Now, inspired by Bloembergen's observation [1] of a power law relation between T_2 and viscosity, Figure 7 plots our fitted T_2's against viscosity. This plot, with a χ^2_R of 1.47, confirms Bloembergen's result regarding a power law for T_2, at least at high viscosity. According to Figure 8, the same might also approximate T_1 reasonably, but the χ^2 suggests that it does not fully capture the behavior–it looks as though the T_1 data has some minor concave curvature, since both endpoints are above the fit and all midpoints below, but it is difficult to tell at the resolution of this data. For further discussion of possible fitting forms for the T_1 data, this author recommends the excellent paper "NMR Relaxation Times of Aqueous Glycerin" by Lucas Orona.

V. T_2 AT LOW CONCENTRATION

Here we resume discussion of the low-concentration anomalies in T_2, as promised. The next feature to add in the model, which might allow us to capture more of the curvature in Figure 6, is typically an $\exp\{-(2\tau/T_D)^3\}$ factor which represents irrecoverable coherence losses due to diffusion. Though fitting with this term does reduce the χ^2_R greatly, we object to its application here because it yields nonphysical fits. Specifically, theory [4] asserts

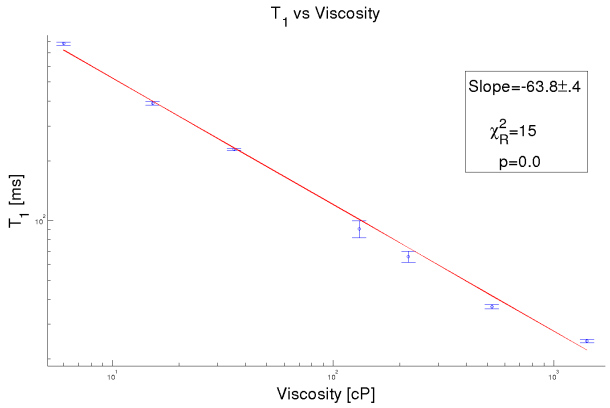

FIG. 8: The T_1-viscosity relation is only approximated by a power law.

that $T_D = \left(\gamma^2 G^2 D/12\right)^{-1/3}$, where γ is the proton gyromagnetic ratio; G is the magnetic field gradient, estimated by moving a gaussmeter around inside the apparatus; and D is a diffusion constant for the aqueous glycerol, obtained from applied chemical research [3]. For our range of parameters, T_D evaluates to a timescale of 10ms, which is far longer than (1) the observation time and (2) the fitted T_D values (hundreds of ms). Additionally, one expects that, as viscosity increases, diffusion should decrease, and T_D should increase; however, our fitted T_D values show precisely the opposite dependance. So we conclude the diffusion factor is not relevant to our T_2 data.

More likely, the problem is that the system was not in thermal equilibrium at the beginning each of the low-concentration T_2 trials. The T_2 experiments were run on repeat from the pulse programmer with an interval of 1s, which does not present a problem for the higher concentration samples. But, as we discovered when doing T_1 measurements (at repeat time 3s), 1s is comparable to the low-concentration T_1 times ($T_1 = 781 \pm 14$ ms for 50% glycerin). If the system has not fully recovered from the previous pulse sequence, we have non-equilibrium initial conditions and expect oddities in our results.

VI. ω_0 AND B DETERMINATIONS

Additionally, we can make use of the sheer quantity of echo measurements taken to determine the Larmor frequency to high precision. On October 26, we collected one hundred echos of the sort shown in Figure 3. Each echo contains roughly twenty peaks, and each peak-to-peak distance provides an estimate of the period of the carrier sinusoid. Examining the estimates from a given echo, we see a random scatter with no obvious structure (eg estimates from the echo center are not noticably different from estimates nearer to edges). We thus take the mean of the period estimates from a given echo, and use the width of the scatter to estimate an uncertainty in that mean.

Then the estimates from each of the hunred echos are combined in an uncertainty-weighted average to arrive at a single estimate of the period, from which we determine the average carrier frequency of our signals. Since, in our experiment, we set $\omega < \omega_0$, we can add our estimated carrier frequency to the ω at which we drove the system to find $\omega_0 = 2\pi \times (7,517,680. \pm 1)$Hz, where the limit on precision is actually the frequency generator readout. Using the known value of γ, we find that our average magnetic field over these runs was $1765.645 \pm .002$G, which agrees with the lab magnetometer ($1750 \pm 20G$).

Now, clearly, the above statistical precision is overkill, since the magnetic field on a given day is not defined to nearly that degree. For a typical gradient of 20G/cm, the tiniest movement of the sample in the apparatus would result in a magnetic field difference much larger than the above uncertainty. However, it is exciting we can measure the magnetic field to the full extent of precision at which it is a well-defined quantity in the experiment.

VII. CONCLUSION

In this paper, we have discussed the theory of NMR and demonstrated the measurement of relaxation times using the Han spin echo. By these means, we have reconfirmed Bloembergen's power-law for the T_2 vs viscosity relation, and found that this relation can only nearly approximate the T_1 curve to the resolution of our data. Then we discussed the utility of this method to precisely determine the magnetic field of the lab NMR setup, which may be useful for future NMR experiments or calibration of the laboratory gaussmeters.

[1] N. Bloembergen, E.M. Purcell, and R.V. Pound. Phys. Rev. 73, 679 (1948).
[2] Dow Chemical Company. http://www.dow.com/optim/optim-advantage/physical-properties.htm
[3] J. Chem. Eng. Data, 2004, 49 (6), pp 1665-1670
[4] H.Y. Carr, and E.M. Purcell. Phys. Rev. 94, 630 (1954).
[5] Bloch, Felix. Phys. Rev. 70, 460.